

# Adsorption by design: tuning atom-graphene van der Waals interactions via mechanical strain

Nathan S. Nichols,<sup>1</sup> Adrian Del Maestro,<sup>1</sup> Carlos Wexler,<sup>2</sup> and Valeri N. Kotov<sup>1</sup>

<sup>1</sup>*Department of Physics, University of Vermont, Burlington, VT 05405*

<sup>2</sup>*Department of Physics and Astronomy, University of Missouri, Columbia, MO 65211*

(Dated: February 16, 2016)

We aim to understand how the van der Waals force between neutral adatoms and a graphene layer is modified by uniaxial strain and electron correlation effects. A detailed analysis is presented for three atoms (He, H, and Na) and graphene strain ranging from weak to moderately strong. We show that the van der Waals potential can be significantly enhanced by strain, and present applications of our results to the problem of elastic scattering of atoms from graphene. In particular we find that quantum reflection can be significantly suppressed by strain, meaning that dissipative inelastic effects near the surface become of increased importance. Furthermore we introduce a method to independently estimate the Lennard-Jones parameters used in an effective model of He interacting with graphene, and determine how they depend on strain. At short distances, we find that strain tends to reduce the interaction strength by pushing the location of the adsorption potential minima to higher distances above the deformed graphene sheet. This opens up the exciting possibility of mechanically engineering an adsorption potential, with implications for the formation and observation of anisotropic low dimensional superfluid phases.

## I. INTRODUCTION

van der Waals (vdW) or dispersion forces play an especially important role at interfaces involving atomically thin materials, such as graphene and structurally similar materials, including transition-metal dichalcogenides (*e.g.* MoS<sub>2</sub>). These can form the building blocks of the so-called van der Waals heterostructures<sup>1</sup>. vdW interactions are fundamentally and practically important, as they reflect the polarization properties of materials and are sensitive to Coulomb interactions. In addition, as will be discussed below, they can depend strongly on material deformations, both through modifications of the electronic structure which affects the polarization, and the changes induced in the electron-electron interactions.

Two-dimensional materials can withstand large strains without rupture, offering unique opportunity for exploration of large strains. In graphene, uniaxial strain effects (most notably along the “armchair” or the “zig-zag” directions) have been studied theoretically within the non-interacting tight-binding framework<sup>2-6</sup>. This theoretical work was mostly motivated by experimental investigations of graphene’s mechanical properties: graphene was confirmed to be the strongest material ever measured<sup>7</sup>, and is able to sustain reversible elastic (uniaxial) strain of  $\delta \approx 20\%$ <sup>8,9</sup>. In addition, strain and ripple formation can coexist and affect the functionalization properties of graphene, such as the adsorption of atomic hydrogen (which quickly turns graphene into an insulator)<sup>10</sup>. One can also imagine many possibilities for local strain engineering, including the creation of strain profiles that can produce desired electronic properties, such as confinement, and surface states.<sup>11</sup> Strain plays an important role in the electronic structure of numerous two-dimensional (2D) materials as described in a recent review (Ref. [12]), and general strain configurations corre-

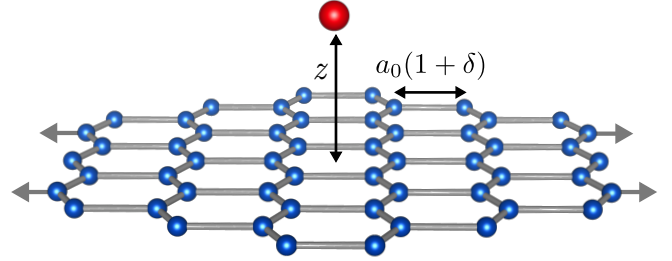


FIG. 1. (Color online) An adatom located a distance  $z$  above a graphene sheet subject to mechanical strain ( $\delta$ ) along the indicated armchair direction.

sponding to gauge fields with different symmetries have to be taken into account. From now on we will consider only uniaxial strain, as it is one of the simplest deformations and is amenable to a practically complete theoretical analysis of vdW forces in terms of their strain and correlation dependence.

The electronic structure under uniaxial strain shows strong directional dependence – in particular, the armchair deformation shown in Fig. 1, results in a tendency towards the system becoming more one dimensional, while a zig-zag stress leads to dimer formation beyond a critical value  $\delta_c \approx 23\%$  which generates a gap (via a topological Lifshitz transition) in the electronic spectrum<sup>2,3</sup>. For weak strain, the electronic spectrum is anisotropic (elliptical, with different Fermi velocities  $v_y \neq v_x$ ) in both cases. This behavior creates a rich variety of possibilities for interplay between strain-induced polarization and electron-electron interactions and is our subject of interest.

Other examples of graphene-based lattices with anisotropic Dirac excitations include: (1) graphene

superlattices<sup>13–16</sup>, (2) tunable honeycomb optical lattices<sup>17</sup>, and (3) molecular graphene, formed by manipulation of carbon monoxide molecules over conventional 2D electron systems<sup>18</sup>. For example, a high anisotropy (ratio of Fermi velocities  $v_y/v_x \approx 0.5$ ) has been achieved in epitaxial graphene modulated on an island superlattice<sup>15</sup>. These recently developed systems provide further opportunities for manipulation and tuning of the conventional graphene electronic structure and thus exploration of the anisotropy-related effects and their consequences for vdW forces.

van der Waals forces between graphene sheets (at distance  $d$ , large enough to eliminate direct hopping between layers), have been a subject of considerable attention<sup>1,19–29</sup>. For Dirac systems in 2D, in particular graphene, the force decreases as fourth power of the distance,  $|F_{vdW}(d)| = C_{vdW}/d^4$ , and is fairly weak compared to relativistic systems (due to the small value of the Fermi velocity compared to the speed of light). A fundamental and practical question arises: *Can this force be enhanced?*

In a recent work<sup>30</sup>, based on the random phase approximation (equivalent to the Lifshitz theory)<sup>31,32</sup>, we have found that the Dirac anisotropy (i.e. strain) can substantially enhance the force resulting from the growth of the polarization with increased anisotropy. Experimentally realizable values of strain show 10 times increases of the force. Moreover, as emphasized in recent works<sup>27,30</sup>, the vdW interaction is very sensitive to the Coulomb coupling and its renormalization; this effect is particularly strong for large strain. Additionally, exchange-correlation phenomena is enhanced in strained graphene, such as the tendency towards itinerant ferromagnetism<sup>33</sup>. The absence of conventional screening of the Coulomb interactions when the Fermi energy is at (or close to) the Dirac point causes strong electron correlation effects in graphene. This is typically the case when graphene is produced, e.g. by mechanical exfoliation<sup>34–38</sup>. The location of the Fermi energy can also be easily shifted to the Dirac point by application of backgate voltage, i.e. due to the strong electric field effect — one of the most important characteristics of the material. A recent overview of interactions in graphene can be found in Ref. [39]. The linear spectrum indicates the effective interaction parameter, typically denoted by  $\alpha = e^2/\hbar v_F$ , is doping independent. For suspended graphene, i.e. without the dielectric screening from a substrate, the coupling reaches its maximum value of  $\alpha \approx 2.2$ .

The main goal of this paper is to investigate how atoms of different types interact with uniaxially strained graphene, which we consider as a prototype strained 2D material. We perform calculations for distances up to 70 nm and restrict ourselves to  $T = 0$  since it is well documented<sup>26,40,41</sup> that finite temperature effects are negligible in this distance range. The study of such atom–2D material interfaces allows us to explore the effects of strain and interactions within the material in their most pure form (since interlayer screening of the

vdW force is not present in this case). While previous works have been devoted to vdW interactions of atoms with isotropic graphene<sup>20,40–44</sup>, our work focuses on the effects of strain and correlations. One of our principal results is that the vdW interaction increases with strain and the relative magnitude of this effect does not depend strongly on the type of atom, i.e. on its mass and polarizability. On the other hand, the vdW interaction is quite sensitive to graphene’s electron-electron interaction coupling constant. Thus, atoms can act as amplifiers of the strain-induced polarization properties of the 2D material, which in turn can lead to profound consequences for the atomic behavior itself near the surface. As an application of our theory we calculate the effect of strain on the quantum reflection amplitude, the probability that a low-energy impinging atom will be reflected from the surface, and find that it can be dramatically reduced.

Increased density of adatoms and the ability to mechanically tune the van der Waals attraction between them and the graphene sheet opens up the possibility of investigating low dimensional collective many-body effects near the surface. The local anisotropy of the deformed graphene lattice structure will strongly affect the physics of adsorption. The search for an ideal and controllable substrate onto which a light gas (H or He) can be adsorbed to form a 2D quantum liquid (or superfluid) has been an area of active research for nearly fifty years.<sup>45</sup> The key requirements for such a substrate include (1) that it is atomically flat and regular, as disorder would tend to localize the fluid and (2) it be only weakly polarizable, to prevent the formation of fully classical wetting layers. Originally, graphite appeared to provide an ideal surface in these regards, and its helium adsorption phase diagram as a function of density and temperature is well understood both experimentally<sup>46–50</sup> and via numerical quantum Monte Carlo simulations<sup>51–53</sup>. It includes a commensurate  $\sqrt{3} \times \sqrt{3}$  R 30° phase (where helium atoms occupy 1/3 of the strong binding sites located at hexagon centers) and possible striped incommensurate and reentrant fluid phases at high densities, but the first adsorbed layer appears to lack any signatures of a more exotic quantum liquid.

While experiments are currently lacking, a single sheet of graphene seems to be an even more appealing substrate for adsorbing quantum fluids as a 10% reduction in the binding energy for a monolayer of helium (compared to graphite) suppresses classical wetting<sup>54</sup>. This idea was explored via a series of recent zero temperature diffusion Monte Carlo studies<sup>55–57</sup> which reported the observation of superfluidity in the first layer of helium on graphene and even the presence of the fleeting *supersolid* phase (where long range off-diagonal and positional order coexist). These results have proven controversial, large scale finite temperature grand canonical quantum Monte Carlo simulations<sup>58</sup> find no evidence of either first layer superfluid response or supersolidity, with the discrepancy being blamed on population size bias in diffusion Monte Carlo<sup>59</sup>. The exact nature of adsorbed

helium on graphene at low temperature thus remains an open question.

The most important ingredient in numerical simulations of helium on graphene is the specific form of the interaction potential between an adsorbate atom and the graphene sheet and is usually taken as a summation of repulsive hard core and attractive van der Waals interactions<sup>60</sup> which may depend on a number of phenomenological parameters. By exploiting our knowledge of the electronic polarizability of the graphene sheet, we have devised a method that enables the independent determination of these parameters by fitting the long distance tail of the van der Waals potential computed within the continuum limit to predictions from the effective microscopic theory. This allows us to investigate both the accuracy of commonly used model parameters for isotropic graphene as well as the effects of strain on their values. We find that while increasing uniaxial strain enhances the long distance van der Waals attraction, it can have the opposite effect at short distances, leading to an overall softening of the adsorption potential with exciting consequences for the energetic feasibility of proximate and possibly anisotropic superfluid phases. These trends are confirmed via *ab initio* calculations of the interaction energy between a helium atom and an aromatic molecule composed of 24 carbon atoms, coronene.

The rest of the paper is organized as follows. In Section II we describe our results for the vdW interaction between uniaxially strained graphene and several types of atoms (with different masses and polarizabilities) as a function of strain and the electron interaction coupling constant. Section III contains results for the elastic quantum reflection (QR) coefficient as a function of strain and Section IV discusses the many-body adsorption potential for helium on strained graphene. In Section V we present our conclusions and perspectives for further exploration.

## II. ATOM-GRAPHENE VAN DER WAALS FORCE

We begin with the problem of strain-dependence of the atom-graphene van der Waals potential. The theory of vdW forces is described in Refs. [26, 31, and 32] and contains, in particular, the fully relativistic treatment within Lifshitz theory, which amounts to the well-known Random Phase Approximation (RPA), including retardation effects incorporated through the polarization function and the interactions. Many works have also been devoted to atom-graphene interactions<sup>20,40–44</sup>. As is well known, and we will see explicitly, relativistic effects depend on the interaction distance and are relatively weak on the nanometer scale (only becoming important on micron scales). Thus we find it useful to write down the (less cumbersome) non-relativistic expressions first, and then include relativistic effects. The zero temperature formalism is used since finite temperature effects are not important in the small distance regime under considera-

tion.

### A. Non-relativistic treatment

The dynamic atomic polarizability  $\alpha(i\omega)$  for various atoms, which is required for the calculation, is known with great precision<sup>61</sup>, and for most atoms can be approximated by the following single-oscillator form (for the vdW force, one needs it on the imaginary axis):

$$\alpha(i\omega) = \frac{\alpha_0 \omega_0^2}{\omega_0^2 + \omega^2}. \quad (1)$$

Here  $\alpha_0$  is the static polarizability. We have performed detailed fits of this form to the data of Ref. [61] for three atoms, and our results are in very good agreement with parameter values quoted in the literature. We obtain, for H:  $\alpha_0 = 4.5$  a.u.,  $\omega_0 = 11.65$  eV; for Na,  $\alpha_0 = 162.6$  a.u.,  $\omega_0 = 2.15$  eV, and for He,  $\alpha_0 = 1.38$  a.u.,  $\omega_0 = 27$  eV. These atoms were chosen because their behavior is relevant to cold atom experiments. Notice that they have very different polarizabilities, where the atomic unit of polarizability is 1 a.u. =  $1.4818 \times 10^{-4}$  nm<sup>3</sup>.

Next, the polarization of the graphene electrons is needed. Assuming uniaxially strained graphene, as shown in Fig. 1, for weak to moderate strain the electronic dispersion is well described by an effective anisotropic Dirac dispersion  $E(\mathbf{k})$  with different, strain-dependent velocities  $v_x, v_y$ <sup>2,4,30</sup>:

$$E(\mathbf{k})^2 = v_x^2 k_x^2 + v_y^2 k_y^2. \quad (2)$$

As mentioned previously, for a lattice deformation in the armchair direction, the system remains semi-metallic (no gap opens) even for strong strain<sup>2,4</sup>. For strain in other directions, in particular in the zig-zag direction, a gap eventually opens as a function of strain, the Dirac cones become severely distorted (merging at the transition point) and cannot be described by Eq. (2). Returning to the case of armchair strain, we have performed a fit to the data described in Refs. [2 and 4], which gives the anisotropy ratio  $v_y/v_x$  as a function of strain  $\delta$ . The relationship between  $v_y/v_x$  and  $\delta$  will be needed in Section IV. We assume strain to be in the  $y$ -direction (armchair direction), reducing the corresponding velocity while the velocity in the perpendicular ( $x$ ) direction is not significantly affected<sup>2,4</sup>. As explained in those works, for small strain  $\delta$  the variation of the velocities is linear, and we find that for the armchair direction is described well by the formulas:  $v_y/v_F = 1 - \Lambda\delta$ ,  $v_x/v_F = 1 + \Lambda\nu\delta$ . Here  $\nu = 0.165$  is the Poisson ratio,  $\Lambda \approx 2.23$ , and  $v_F$  is the velocity of unstrained graphene. Beyond weak ( $\approx 10\%$ ) strain, the dependence on strain becomes (only weakly) nonlinear, and the above formulas continue to approximately describe the numerical results<sup>4</sup> even for moderately strong deformations. After taking into account the weak non-linearity in the armchair direction, we arrive

at the correspondence between velocity anisotropy and strain shown in Table I.

$v_y/v_x$	1.00	0.75	0.40	0.20
$\delta$	0.00	0.10	0.25	0.34

TABLE I. The relationship between the Fermi velocity anisotropy and the elongation of the  $y$ -axis of a strained graphene lattice using data inferred from Refs. [2 and 4].

For the rest of this section we will vary the effective Dirac anisotropy  $v_y/v_x$  from 1 (isotropic graphene) down to its largest value of 0.2 and we introduce the notation:

$$v_{\perp} \equiv \frac{v_y}{v_x} \leq 1. \quad (3)$$

We consider graphene at half-filling, i.e. the chemical potential is at zero (the lower Dirac cone is full, the upper one is empty). Returning to the calculation of the polarization, a simple rescaling of the isotropic graphene case leads to the exact expression<sup>30</sup>:

$$\Pi(\mathbf{q}, i\omega) = -\frac{1}{4v_x v_y} \frac{v_x^2 q_x^2 + v_y^2 q_y^2}{\sqrt{v_x^2 q_x^2 + v_y^2 q_y^2 + \omega^2}}. \quad (4)$$

From here, the vdW energy in the non-relativistic limit is<sup>26</sup>:

$$U_{\text{vdW}}(z) = -\frac{\hbar}{2\pi} \int_0^{\infty} d\xi \alpha(i\xi) 2 \int_0^{\infty} dk k^2 e^{-2kz} \times \int_0^{2\pi} \frac{d\phi}{2\pi} \frac{|V(\mathbf{k})\Pi(\mathbf{k}, i\xi)|}{1 - V(\mathbf{k})\Pi(\mathbf{k}, i\xi)}. \quad (5)$$

This is the RPA result. Here  $\phi$  is the angle between the  $k_x$  and  $k_y$  directions (in the strained case there is an explicit angular dependence). The Coulomb potential is:

$$V(\mathbf{k}) = \frac{2\pi e^2}{k}, \quad k = |\mathbf{k}|. \quad (6)$$

Finally, we define graphene's dimensionless coupling constant  $g$  as:

$$g = \frac{\pi e^2}{2 v_x} \quad (7)$$

where we have set  $\hbar = 1$ . The value in vacuum can be obtained by noting that for graphene  $e^2/v_x \approx 2.2$ ,<sup>39</sup> leading to  $g \approx 3.45$ . If graphene is placed on a substrate (and one assumes vacuum in the upper half-space), the effective charge  $e^2$  decreases due to the dielectric constant,  $\kappa$ , of the substrate and we have to replace  $e^2 \rightarrow 2e^2/(1+\kappa)$ . For example, a SiO<sub>2</sub> substrate has  $\kappa \approx 4$  and the coupling  $g$  decreases substantially<sup>39</sup>.

Returning to Eq. (5), the vdW potential can be conveniently expressed as:

$$U_{\text{vdW}}(z) = -\frac{C_3(z)}{z^3}, \quad (8)$$

where:

$$C_3(z) = \frac{\alpha_0 \omega_0}{8\pi} \frac{g}{v_{\perp}} \int_0^{\infty} \frac{d\omega}{1 + \omega^2} \int_0^{2\pi} \frac{d\phi}{2\pi} \int_0^{\infty} dq q^3 e^{-q} \times \frac{f(\phi, v_{\perp})}{\sqrt{q^2 f(\phi, v_{\perp}) + \omega^2 \Omega^2} + (g/v_{\perp}) q f(\phi, v_{\perp})}. \quad (9)$$

Here we have written the result in such a way that the physical dimension of  $C_3$  comes only from the pre-factor  $\alpha_0 \omega_0$ , while the other couplings and the integration variables  $q, \omega$  are dimensionless. We also use the definition:

$$f(\phi, v_{\perp}) = \cos^2 \phi + v_{\perp}^2 \sin^2 \phi. \quad (10)$$

The characteristic dimensionless scale  $\Omega$  is defined as

$$\Omega = \Omega(z) \equiv \frac{2\omega_0 z}{v_x}, \quad (11)$$

and is distance-dependent.

## B. Relativistic effects

The above formulas are generalized to take into account relativistic corrections in full, which enter in two ways. First, there is an explicit contribution from retarded potential pieces<sup>20,26,31,32,40,41</sup>, proportional to  $(v_x/c)^2 = (1/300)^2 \ll 1$ , which can be safely neglected. Second, there is a retardation modification of the Coulomb interaction portion, which now reads (as before, all integration variables are dimensionless)

$$C_3(z) = \frac{\alpha_0 \omega_0}{8\pi} \frac{g}{2v_{\perp}} \int_0^{\infty} \frac{d\omega}{1 + \omega^2} \int_0^{2\pi} \frac{d\phi}{2\pi} \int_{\omega_c \omega}^{\infty} dq q^3 e^{-q} \times \frac{f(\phi, v_{\perp}) \times \left(2 - \frac{\omega_c^2 \omega^2}{q^2}\right)}{\sqrt{q^2 f(\phi, v_{\perp}) + \omega^2 \Omega^2} + (g/v_{\perp}) q f(\phi, v_{\perp})}, \quad (12)$$

where we introduce the relativistically generated dimensionless, distance-dependent scale, which in particular provides an effective cutoff in the above integration:

$$\omega_c \equiv \Omega(z)/(c/v_x) = \Omega(z)/300. \quad (13)$$

The non-relativistic formula is recovered for  $\omega_c = 0$  ( $c = \infty$ ). It is clear that for finite speed of light  $c$  the relativistic effects become more important as the distance,  $z$ , increases (so that  $\omega_c$  starts deviating substantially from 0). At very large  $z$ , within the regime  $\omega_c > \Omega$ ,  $C_3(z) \sim 1/z$ , i.e. the vdW potential changes shape. Our approach above is equivalent (apart from different notation) to the conventionally used Lifshitz theory<sup>26,31,32</sup>, and the  $C_3$  results for isotropic graphene are completely consistent with published numbers for H, He, Na<sup>20,40-44</sup>.

Now, we proceed to a more detailed discussion of our results as a function of strain (Dirac cone anisotropy). First we show that  $C_3(z)$  generically has substantial distance dependence, which is already present in the non-relativistic limit, Eq. (9), due to the frequency dependence (semi-metallic nature) of graphene's polarization.

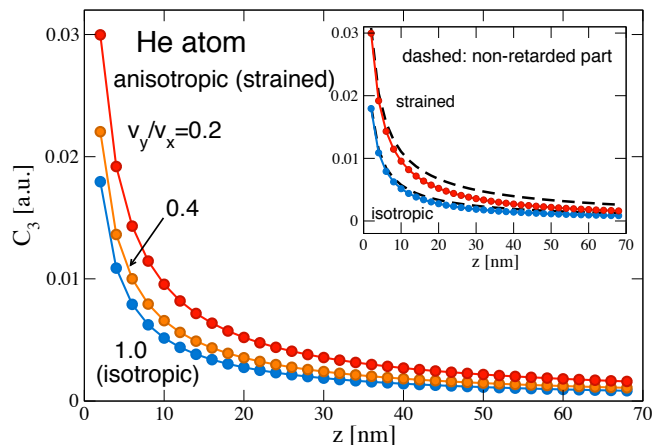


FIG. 2. (Color online) Distance dependence of  $C_3(z)$  which determines the vdW potential via Eq. (8). Results are plotted for a He atom, for several values of the anisotropy  $v_{\perp} = v_y/v_x$ . Inset: Comparison of the fully relativistic expression with the non-relativistic formula (dashed lines) for the isotropic ( $v_{\perp} = 1$ ) and maximally strained ( $v_{\perp} = 0.2$ ) cases.

A comparison of Eq. (9) with the fully relativistic expression Eq. (12) is presented in Fig. 2 (inset), for He. The difference between the two is appreciable (even in the nm distance range), and increases with distance, as expected.

Therefore, in order to achieve maximum accuracy, from now on we will use the fully relativistic formula Eq. (12). The main panel in Fig. 2 shows the dependence of  $C_3$  on the anisotropy  $v_{\perp}$  for He. We assume, for definitiveness, that graphene is free-standing (in vacuum) i.e. the electron-electron coupling is  $g = 3.45$ . Atomic units of  $C_3$  are defined as: 1 a.u. of  $C_3 = 4.032 \text{ meV nm}^3$ . We find a significant dependence on strain, which tends to increase the value of  $C_3$ . This increase can be traced to the enhancement of the electron polarization from Eq. (4) with strain. A factor of 2 increase in the vdW potential is seen for almost all distances at the maximal strain under consideration ( $v_{\perp} = 0.2$ ). Finally, the shape of the curves in Fig. 2 suggests that the vdW potential experiences significant deviations from a pure  $1/z^3$  tail, even at such intermediate (nm) distances. We will analyze this crossover at the end of this Section.

In Fig. 3, we present our results for H and Na atoms. Even though the scales of  $C_3$  differ significantly, due to the very different atomic polarizabilities (Na is approximately forty times more polarizable), the overall anisotropic behavior for these atoms is quite similar. It is also similar to the case of (weakly polarizable) He shown in Fig. 2.

In Fig. 4, we plot results for the combined effect of anisotropy and electron-electron interaction  $g$ . The interaction controls both the overall scale of  $C_3$  and (metallic) screening, as reflected in the denominator of Eq. (12). If screening were absent, the strain dependence of  $C_3$  would

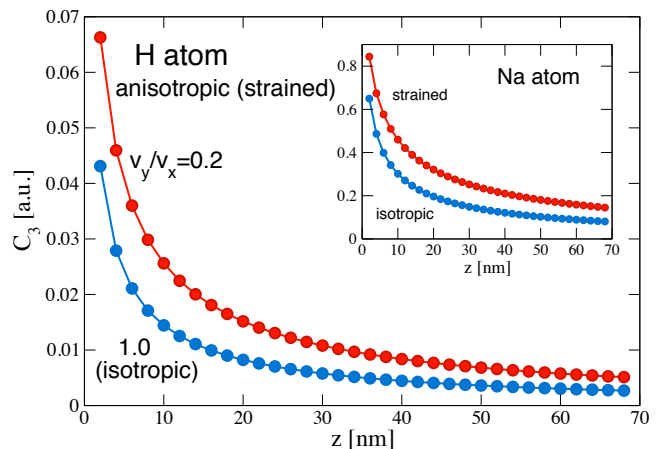


FIG. 3. (Color online) Distance dependence of  $C_3(z)$  which determines the vdW potential via Eq. (8), for H atom on isotropic ( $v_{\perp} = 1$ ) and maximally strained graphene ( $v_{\perp} = 0.2$ ). Inset: Same as main panel, for a Na atom; note the larger vertical scale.

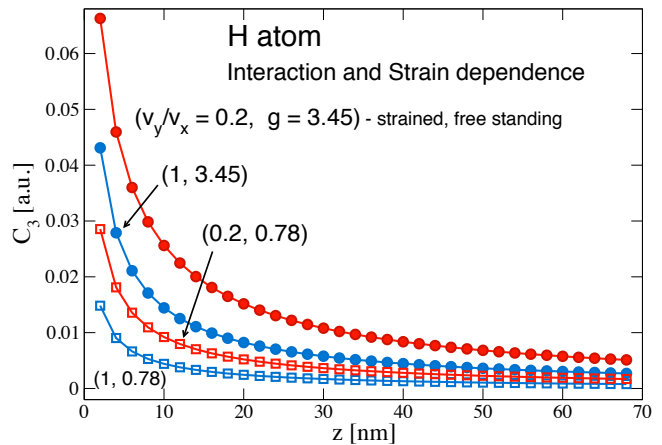


FIG. 4. (Color online) Combined correlation ( $g = (\pi/2)(e^2/v_x)$ ) and anisotropy ( $v_{\perp}$ ) dependence of  $C_3(z)$  for a H atom. The representative electron interaction values correspond to  $e^2/v_x = 2.2$  (vacuum), and  $e^2/v_x = 0.5$  (screened case).

be much more pronounced. This effect is only marginally visible in Fig. 4, i.e. the increase of  $C_3$  is slightly larger for  $g = 0.78$  (lower two curves) than for  $g = 3.45$  (upper two curves). The overall reduction of the vdW interaction as  $g$  decreases is the dominant behavior.

Finally, we examine the crossover in the distance dependence of the potential. The significant  $z$ -dependence of  $C_3(z)$  suggests a fit of the form  $C_3(z) = C_4/(z + L)$ , where  $C_4$  and  $L$  are the fitting parameters. In standard atomic units, 1 a.u. of  $C_4 = 4.032 \text{ meV nm}^4$ . Our results for all studied atoms are summarized in Fig. 5. We find that the crossover distances are in the nm distance region, and increase with strain. For He and H we have

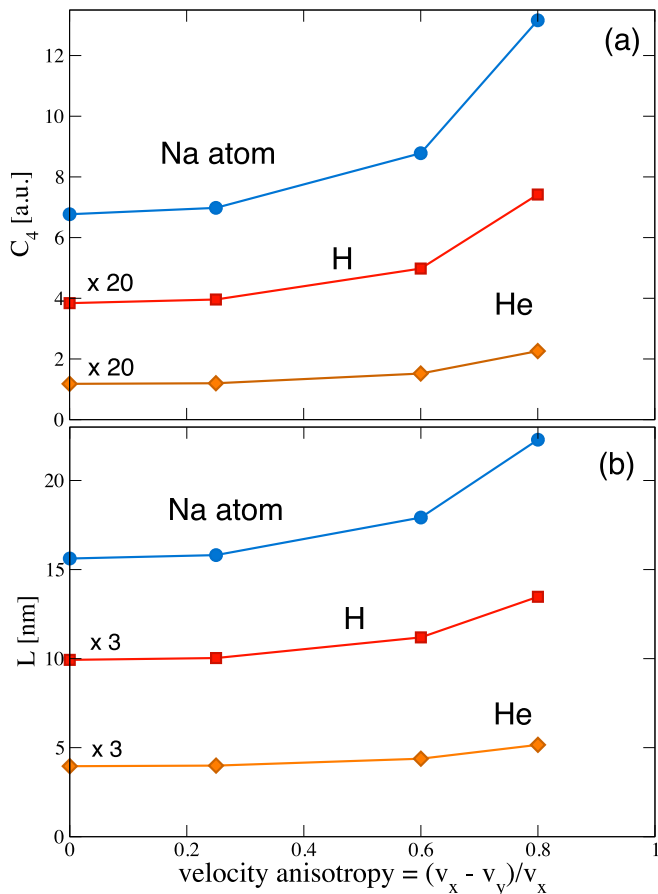


FIG. 5. (Color online) Crossover from  $C_3/z^3$  to  $C_4/z^4$  behavior in the vdW potential tail, as a function of the anisotropy  $(1 - v_\perp)$ . Fits are performed to the expression  $C_3(z) = C_4/(z + L)$  with panel (a) showing  $C_4$  and (b) the value of the crossover lengthscale  $L$ .

$L \simeq 1.3, 3.3$  nm respectively, for isotropic graphene, while the corresponding value for Na is significantly larger,  $L \simeq 15.6$  nm. Thus at distances  $z \gg L$  the vdW potential becomes  $U_{\text{vdW}}(z) = -C_4/z^4$ . The coefficient  $C_4$  also increases with strain as shown in Fig. 5.

### III. IMPLICATIONS FOR QUANTUM REFLECTION

As a first application of our results, we consider the strain dependence of the quantum reflection (QR). For elastic interactions, ultracold atoms impinging on graphene should be subject to quantum reflection from the attractive vdW tail of the atom-graphene potential. QR is a simple result of the wave-like nature of low-energy particles moving in an attractive potential that falls off sufficiently rapidly with distance from the surface. Under QR, an ultracold atom can have a high probability of reflecting without ever reaching a classical turning point

near the graphene surface. Studied since the development of quantum mechanics, QR continues to fascinate both theorists<sup>62–64</sup> and experimentalists<sup>65–67</sup> alike and while QR has been previously studied for graphene<sup>62</sup>, we now investigate the effect of uniaxial graphene strain on its properties. Since we have found in the previous Section that the vdW potential is sensitive to the Dirac anisotropy, this implies that QR might be efficiently tuned with uniaxial strain.

To determine how the vdW potential affects above-barrier quantum reflection (see e.g. Refs. [68 and 69] for an overview) we consider a non-relativistic atom with energy  $E = \hbar^2 k^2 / (2M)$  and mass  $M$  impinging on graphene (where we have temporarily restored  $\hbar$  for clarity). The behavior of the QR reflection coefficient  $R$ , defined as the magnitude of the reflectivity (i.e. the piece of the wavefunction which is reflected), depends on the distance dependence of  $U_{\text{vdW}}(z)$ . In the regime under consideration where  $U_{\text{vdW}}(z)$  experiences a crossover from  $-C_3/z^3$  to  $-C_4/z^4$  behavior, the value of the effective parameter  $\rho$  determines which part of the tail is the dominant contribution to  $R$ :<sup>68</sup>

$$\rho = \frac{\sqrt{2M}}{\hbar} \frac{C_3}{\sqrt{C_4}}, \quad (14)$$

where  $C_4$  is determined from Fig. 5 and the constant  $C_3$  is defined as  $C_3 \equiv C_4/L$ . In the low-energy regime, if  $\rho \ll 1$ , then the  $-C_3/z^3$  part determines  $R$ , while  $\rho \gg 1$  means that the  $-C_4/z^4$  tail is more important. Taking into account our results from Fig. 5, we find the following numbers for different atoms (for isotropic graphene):  $\rho_{\text{H}} \approx 1.9$ ,  $\rho_{\text{He}} \approx 5.2$  and  $\rho_{\text{Na}} \approx 11.2$ . The value for H is the smallest, resulting from its small atomic mass. From the results of Ref. [68], we can see that the value of  $\rho$  that separates the asymptotically small and large values is around  $\rho \approx 3$ .

Let us consider, for definitiveness, the case of Na, where the  $-C_4/z^4$  tail is dominant, and estimate the effect of strain on  $R$ . It is convenient to define<sup>68</sup> the length scale  $\beta_4$  via:

$$U_{\text{vdW}}(z) = -\frac{C_4}{z^4} \equiv -\frac{\hbar^2}{2M} \frac{\beta_4^2}{z^4}, \quad (15)$$

such that

$$\beta_4 = \frac{\sqrt{2MC_4}}{\hbar}. \quad (16)$$

The asymptotic behavior of  $R$  in the low-energy region  $E \rightarrow 0$ , or in proper dimensionless units,  $\beta_4 k \ll 1$ , is then:<sup>68</sup>

$$R \approx 1 - 2(\beta_4 k), \quad \beta_4 k \ll 1. \quad (17)$$

In the opposite, high-energy regime, we have:

$$R \sim e^{-1.694\sqrt{\beta_4 k}}, \quad \beta_4 k \gg 1, \quad (18)$$

which is valid, provided  $1 \ll \beta_4 k \ll \rho^2$ .<sup>68</sup>

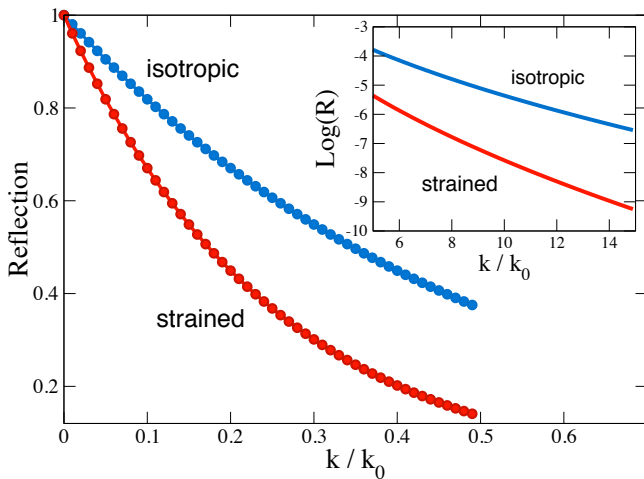


FIG. 6. (Color online) Asymptotic behavior of the quantum reflection coefficient  $R$  for unstrained graphene and anisotropic (strained) graphene with  $v_{\perp} = 0.2$ , in the regime where the tail  $-C_4/z^4$  dominates, as a function of the atomic momentum  $k$ . The length scale is defined as  $1/k_0 \equiv \beta_4$ . In the main panel the low energy behavior is plotted. Inset: High energy behavior, corresponding to exponentially small reflection.

Since  $C_4$  (and therefore  $\beta_4$ ) increases with strain, (see Fig. 5), it is clear that larger strain leads to a decrease of the quantum reflection, as shown in Fig. 6. This decrease of the QR can be very substantial (for moderately large strain). Finally, in situations where the  $-C_3/z^3$  piece of the vdW tail dominates, the corresponding asymptotic behavior is also well established<sup>68</sup> and the strain dependence can be readily calculated, leading to behavior qualitatively very similar to the one in Fig. 6.

Having understood that uniaxial strain enhances the van der Waals interaction between an impinging atom and a deformed graphene substrate, thus leading to a marked reduction in the probability of its reflection, we now ask what effects it may have *near* the surface. In particular, we investigate the physics of adsorption of light atoms onto mechanically strained graphene.

#### IV. HELIUM-4 ADSORPTION POTENTIAL

In this section we focus exclusively on the interaction between a single  $^4\text{He}$  atom and graphene, but the techniques we develop could be applied to the study of adsorption of any neutral polarizable atom.

One conventional treatment of helium adsorption on graphene (or a graphite surface)<sup>60</sup> estimates the total potential energy  $U(\mathbf{r})$  for a neutral adatom at position  $\mathbf{r} = (x, y, z)$  as a discrete summation of Lennard-Jones (6–12) two-body interactions with the  $N$  carbon atoms

located at  $\mathbf{R}_i = (X_i, Y_i, 0)$ :

$$U(\mathbf{r}) = 4\varepsilon \sum_{i=1}^N \left[ \left| \frac{\sigma}{\mathbf{r} - \mathbf{R}_i} \right|^{12} - \left| \frac{\sigma}{\mathbf{r} - \mathbf{R}_i} \right|^6 \right]. \quad (19)$$

We note that the adatom experiences the effects of a corrugated graphene sheet at short distances and thus the potential is a function of the full spatial coordinate  $\mathbf{r}$  as opposed to the continuum approximation used in Eq. (8) where it is only sensitive to the height  $z$  above the sheet. The  $r^{-12}$  form of the short distance interaction is semi-empirical and is meant to capture the effects of Pauli repulsion from overlapping electronic orbitals, while the  $r^{-6}$  attractive part of Eq. (19) is due to the individual vdW dispersion forces between the neutral carbon and helium atoms. For two interacting atoms, the Lennard-Jones (LJ) parameters  $\sigma$  and  $\varepsilon$  set the location of the minimum at  $r_m = 2^{1/6}\sigma$  and its depth at  $-\varepsilon$ . For pure gases and liquids, they can be estimated using second-virial or viscosity coefficients<sup>70</sup> whereas for mixtures, they can be roughly approximated<sup>71</sup> using the Lorenz-Bertholot mixing rules, which for two species  $A$  and  $B$  are given by:

$$\begin{aligned} \varepsilon_{A-B} &= \sqrt{\varepsilon_A \varepsilon_B} \\ \sigma_{A-B} &= \frac{\sigma_A + \sigma_B}{2}. \end{aligned} \quad (20)$$

For a single helium atom interacting with carbon in either graphene or graphite, the most commonly used parameters are taken from Ref. [60] to be  $\varepsilon_{\text{He-C}} = 16.2463$  K and  $\sigma_{\text{He-C}} = 2.74$  Å. These values were determined by comparing the bound states of Eq. (19) to experimental results for the adsorption spectra of helium on graphite<sup>72</sup>. It is thus natural to ask if these LJ parameters can be used to capture the effects of strain considered in the previous sections within the continuum approximation and shown in Fig. 2. The answer to this question constitutes the remainder of this paper.

##### A. Unstrained graphene

We begin our analysis by investigating the accuracy of the Lennard-Jones potential for helium interacting with an isotropic graphene sheet by comparing Eq. (19) with the long-distance continuum limit value  $U_{\text{vdW}}(z) = -C_3(z)/z^3$  in Eq. (8). In Fig. 7 we show the adsorption potential for  $N = 2^{18}$  carbon atoms using the standard LJ parameters for He-C interactions as a function of distance above the graphene sheet for the three high symmetry locations  $\mathbf{r}_A = (0, 0, z)$ ,  $\mathbf{r}_B = (\sqrt{3}a_0/2, 0, z)$  and  $\mathbf{r}_C = (\sqrt{3}a_0/2, a_0/2, z)$ , shown in the upper left inset. Here  $a_0 = 1.42$  Å is the isotropic C-C bond length. The main panel depicts the usual form of the LJ adsorption potential at short distances, with the details of the attractive minima and hardcore repulsion depending on the relative orientation of the adatom with respect to the graphene lattice<sup>73</sup>. For distances  $z > 10$  Å, the potential is insensitive (at the order of  $10^{-10}$  K) to the  $x$

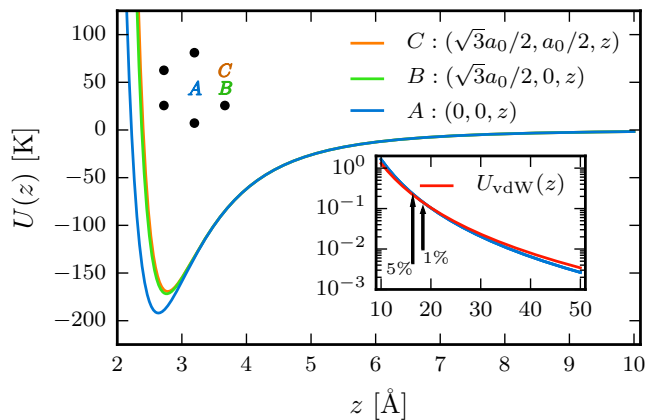


FIG. 7. (Color online) The Lennard-Jones potential for a single helium atom located a distance  $z$  above a graphene sheet at positions  $A, B, C$  (shown in upper left) using  $\varepsilon_{\text{He-C}} = 16.2463$  K and  $\sigma_{\text{He-C}} = 2.74$  Å. The inset (same axes) shows a comparison with the long distance van der Waals potential computed using the continuum polarization of the graphene sheet. Arrows indicate the values of  $z$  where the relative error between the two calculations is 5% and 1% respectively.

and  $y$  positions of the adatom and the substrate can be effectively treated in the continuum approximation. The inset shows  $U(\mathbf{r}_A)$  along with the continuum long distance calculation  $U_{\text{vdW}}(z)$  for He from Section II B with the relative error decreasing from 5% at  $z \simeq 16$  Å to 1% at  $z \simeq 18$  Å. We stress that this agreement is achieved with no adjustable parameters and serves as an excellent benchmark of our continuum calculations at long distances.

### B. Lennard-Jones parameters for strained graphene

In Section II we found that the dispersion force between adatoms and graphene *increases* at long distances as a function of increasing mechanical strain. This finding can be investigated by evaluating the discrete LJ potential for graphene lattices with strain  $\delta = 0.0, 0.1, 0.25, 0.34$  defined as the relative elongation of the lattice along the armchair direction and corresponding to the velocity anisotropies  $v_y/v_x$  considered above and shown in Table I. For each value of the strain parameter  $\delta$  we construct a graphene lattice consisting of  $N = 2^{18}$  atoms in the  $z = 0$  plane with positions defined by the lattice:

$$\begin{aligned} \mathbf{a}_1 &= \frac{\sqrt{3}a_0}{8}(4 + \delta - 3\delta\nu, \sqrt{3}(4 + 3\delta - \delta\nu)) \\ \mathbf{a}_2 &= \frac{\sqrt{3}a_0}{8}(-4 - \delta + 3\delta\nu, \sqrt{3}(4 + 3\delta - \delta\nu)) \end{aligned} \quad (21)$$

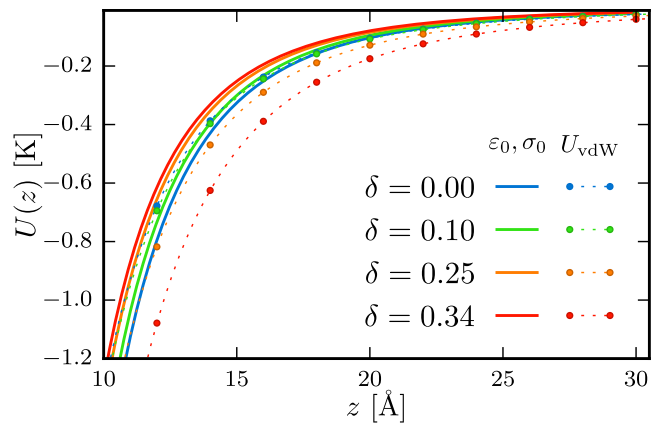


FIG. 8. (Color online) The long distance tail of the adsorption potential for a He adatom as a function of the height above a graphene sheet subject to mechanical strain parametrized by  $\delta$ . Solid lines show the results of the discrete Lennard-Jones potential  $U(z)$  using the standard parameters  $\varepsilon_0, \sigma_0$  given in the text, while points connected by dashed lines show  $U_{\text{vdW}}(z)$  computed within a continuum approximation. Note that the two methods show the opposite strain dependence indicating the failure of the standard Lennard-Jones calculation for strained graphene.

and basis vectors:

$$\begin{aligned} b_1 &= (0, 0) \\ b_2 &= a_0(0, 1 + \delta) \end{aligned} \quad (22)$$

where  $\nu = 0.165$  is the Poisson ratio for graphite<sup>2</sup>.

For distances beyond 1 nm, a comparison of the discrete and continuum calculations for the potential for different strains  $\delta$  is shown in Fig. 8 where we have again used the standard LJ parameters for He-C, now labeling them  $\varepsilon_0 \equiv \varepsilon_{\text{He-C}}$  and  $\sigma_0 \equiv \sigma_{\text{He-C}}$ . Not only do we find considerable disagreement away from  $\delta = 0$ , but the strain dependence has opposite signs; the discrete calculation yields weaker dispersion forces as the strain is increased. This finding indicates that the isotropic LJ parameters for He-C interactions cannot be used when computing the adsorption potential for strained graphene lattices. This failure is perhaps unsurprising, as these effective parameters are meant to capture a plethora of microscopic details that are certainly strain dependent.

To address this fundamental discrepancy we have devised a procedure that allows us to determine the strain dependence of  $\varepsilon$  and  $\sigma$ . We proceed by constructing a set of strained finite size graphene lattices, then compute the potential energy  $U(z) \equiv U(0, 0, z)$  using the brute-force discrete summation in Eq. (19) for a fine mesh of LJ parameters  $\varepsilon \in \{0.9\varepsilon_0, \dots, 1.1\varepsilon_0\}$  and  $\sigma \in \{0.9\sigma_0, \dots, 1.1\sigma_0\}$  with the expectation that the values of strain under consideration should not have an  $O(1)$  effect. The resulting four dimensional data set:  $U(z; \varepsilon, \sigma, \delta)$  can then be compared with the long distance continuum value of  $U_{\text{vdW}}(z; \delta)$  using the mean squared



residual:

$$\chi^2(\varepsilon, \sigma, \delta) = \sum_{i=1}^n |U(z_i; \varepsilon, \sigma, \delta) - U_{\text{vdW}}(z_i; \delta)|^2 \quad (23)$$

for  $n = 3364$  values of  $z$  in the range  $z = 16.37 - 50 \text{ \AA}$ . The starting point for the residual calculation of  $z_0 = 16.37 \text{ \AA}$  was chosen such that the relative error between the long distance potential and the discrete summation was equal to 5% for  $\delta = 0$  (Fig. 7 inset). Although this choice is somewhat arbitrary, we found little dependence on the final results when choosing  $z_0 = 18.40 \text{ \AA}$  corresponding to a 1% relative error for isotropic graphene. We were, however, limited to single precision as all computations were performed on graphical processing units to reduce their run time. No finite-size effects were observed at this level for graphene lattices with  $N \geq 2^{18}$  carbon atoms.

The residual  $\chi^2$  is minimized by the two-parameter function  $\varepsilon(\sigma, \delta)$  over the range of parameters considered and we must add an additional constraint in order to extract the optimal values of  $\varepsilon$  and  $\sigma$  for a given strain. This can be accomplished by requiring that the  $\delta$ -dependent LJ parameters are *close* to the isotropic ones  $\varepsilon_0$  and  $\sigma_0$ . To this end, we define a relative Euclidean distance-cost function:

$$\Delta^2(\varepsilon, \sigma, \delta) = \left( \frac{\varepsilon}{\varepsilon_0} - 1 \right)^2 + \left( \frac{\sigma}{\sigma_0} - 1 \right)^2 \quad (24)$$

and search for the global minimum of the “fit-likelihood” estimator

$$\mathcal{S}(\delta) = \frac{\chi^2}{\max_{\varepsilon, \sigma} \chi^2} + \frac{\Delta^2}{\max_{\varepsilon, \sigma} \Delta^2} \quad (25)$$

with the results displayed in Fig. 9. The global best fit values (including those for isotropic graphene) are indicated with a star and their explicit values are given in Table II. Again there is flexibility in the specific form of the

$\delta$	0.00	0.10	0.25	0.34
$\varepsilon$ [K]	16.247(7)	16.28(9)	16.407(6)	16.61(2)
$\sigma$ [ $\text{\AA}$ ]	2.739(7)	2.782(8)	2.895(6)	3.08(1)

TABLE II. The optimal values of the Lennard-Jones parameters which best reproduce the long distance continuum van der Waals tail of the adsorption potential for a helium atom above strained graphene. The uncertainty in the final digit is indicated in parenthesis where the error can be attributed to the starting position height  $z_0$  of the residual  $\chi^2$  and the functional form of the cost-distance function  $\Delta^2$

likelihood estimator  $\mathcal{S}(\delta)$  in Eq. (25) and we have investigated the effects of using other functions, including different weightings of  $\varepsilon$  and  $\sigma$  as well as a relative scale factor between  $\chi^2$  and  $\Delta^2$ . These ambiguities add an additional

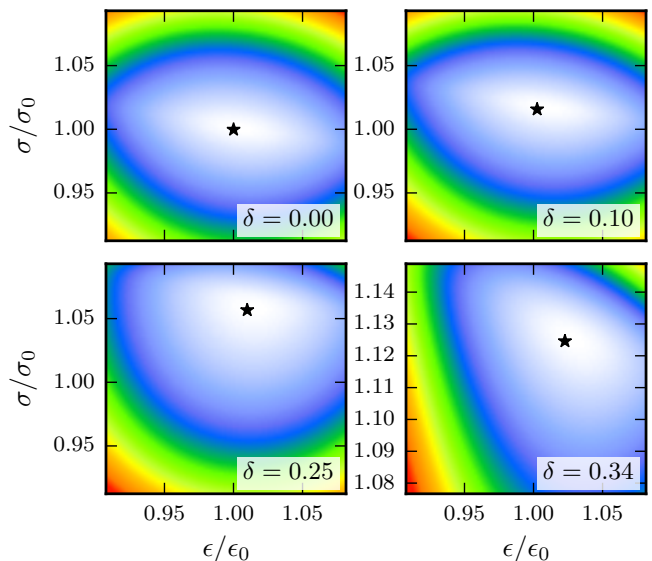


FIG. 9. (Color online) The likelihood estimator  $\mathcal{S} \sim \chi^2 + \Delta^2$  defined in Eq. (25) used to determine the value of the Lennard-Jones parameters  $\varepsilon$  and  $\sigma$  producing the best fit to the long distance continuum van der Waals potential for a single helium-4 atom above strained graphene with  $\delta = 0, 0.1, 0.25$  and  $0.34$ . Axes are normalized to the conventionally employed interaction parameters for helium and carbon:  $\varepsilon_0 = 16.2463 \text{ K}$  and  $\sigma_0 = 2.74 \text{ \AA}$  with the density scale indicating the goodness of fit from light (best) to dark (worst). The star indicates the identified global best fit.

source of error (along with the starting  $z$ -coordinate of the residual) that is reflected in the quantitative uncertainties reported in Table II. These errors, which are on the order of a few percent, do not affect the observed qualitative dependence on strain: both Lennard-Jones parameters are monotonically increasing functions of  $\delta$ .

We note, rather remarkably, that for isotropic graphene, we recover the experimentally determined parameters  $\varepsilon_0$  and  $\sigma_0$  used for helium interacting with a graphite surface<sup>60</sup>. This result provides a novel and independent theoretical verification of the validity of these parameters, as the inputs to our calculation only include the dynamical polarizability of helium defined in Eq. (1) and the well known properties of graphene in vacuum.

As strain is increased, both  $\varepsilon$  and  $\sigma$  grow, with  $\sigma$  being most strongly affected, (increasing by over 10% for  $\delta = 0.34$ ). This is the expected behavior, as it encapsulates the geometric properties of the potential and sets the distance at which the attractive minima occurs for a two-body interaction.  $\varepsilon$ , which sets the energy of the minimum, increases by 2.5% at the highest strain considered. This different response to strain is likely indicative of their role in the potential, Eq. (19), where  $\varepsilon$  sets a linear scale while  $\sigma$  appears with the sixth power of the distance and thus has a greater effect on the long distance tail.

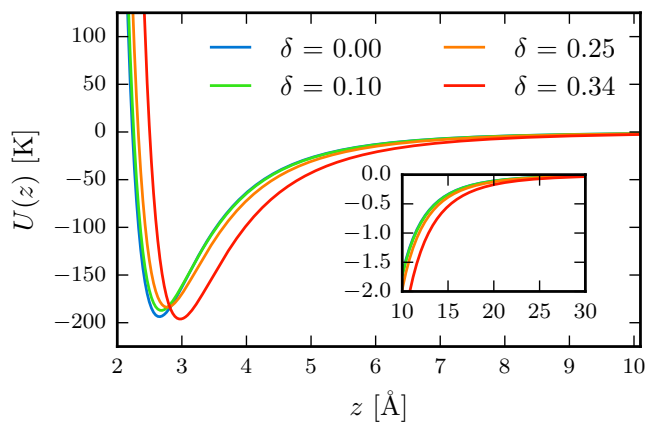


FIG. 10. (Color online) The Lennard-Jones adsorption potential for a He adatom placed at coordinate  $\mathbf{r}_A = (0, 0, z)$  above a graphene sheet with uniaxial strain along the arm-chair direction parameterized by  $\delta$ . The inset (same axes) shows the long distance tail of the potential, with increasing strain causing the dispersion force to increase, in agreement with continuum van der Waals calculations in the long distance limit.

### C. Results: strained Lennard-Jones potential

Having determined the strain dependent Lennard-Jones parameters in Table II we now compute the complete form of the many-body adsorption potential for a He adatom above strained graphene, with the results shown in Fig. 10. Here the helium atom is centered with respect to the hexagonal graphene unit cell ( $\mathbf{r}_A = (0, 0, z)$ ), as in Fig. 7) and we observe that the location of the attractive minima,  $r_m$  is pushed to larger distances above the sheet as the strain increases, with a concomitant softening (increase) of the potential from  $U(r_m) \simeq -192$  K for isotropic graphene with  $\delta = 0$  to  $U(r_m) \simeq -182$  K at  $\delta = 0.25$ . For the strongest strain,  $\delta = 0.34$ , we find that the location of minima is pushed out to a distance of  $r_m \simeq 2.95$  Å, but in contrast to weaker strain, its depth decreases to  $U(r_m) \simeq -194$  K indicating a propensity for enhanced adsorption. We believe that this behavior may be indicative of a breakdown of our fitting procedure at large strain as it only weights deviations in the long distance tail and neglects the corrugated structure of the lattice at short distances. This is confirmed in the next section via ab-initio calculations. During the fit, the large increase of the vdW force found in the continuum approximation at large strain is most efficiently captured through an increase in  $\sigma$ . For two particles, changes in  $\sigma$  only alter the location of the potential minimum, whereas the maximum depth of the many-body adsorption potential is strongly dependent on this hard-core radius as well as the relative coordination between the adatom at the graphene lattice as seen in Fig. 7.  $\epsilon$ , on the other hand, has the same effect on both the two- and many-body potential, setting an overall lin-

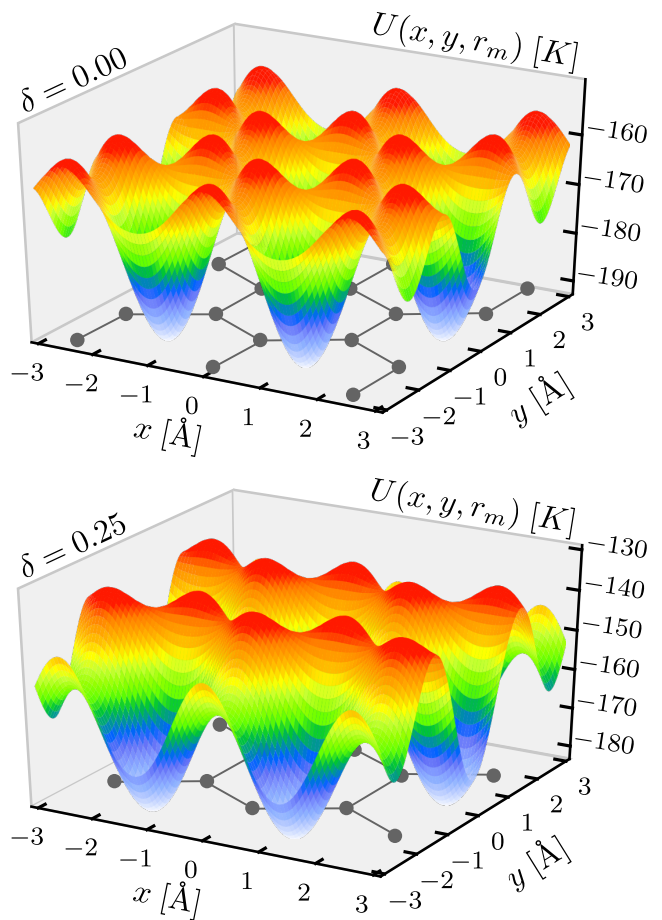


FIG. 11. (Color online) The spatial dependence of the Lennard-Jones adsorption potential for a He atom at a fixed distance  $z = r_m(\delta)$  above an isotropic ( $\delta = 0$ , top) and strained ( $\delta = 0.25$ , bottom) graphene sheet using the parameters in Table II.

ear energy scale.

To better understand these effects, we fix  $z = r_m(\delta)$  and evaluate the adsorption potential  $U(x, y, r_m)$  as a function of the  $x$  and  $y$  coordinates as seen in Fig. 11. For unstrained graphene (top panel), we observe modulations on the order of 15% as the atom is moved laterally at fixed  $z$ . The potential has an egg-carton structure with global minima occurring at hexagon centers and giving rise to the  $\sqrt{3} \times \sqrt{3}$  R30° commensurate phase experimentally observed in graphite<sup>46,47,49</sup>. This phase, where helium atoms occupy 1/3 of the strong binding sites, has also been observed for isotropic graphene in Monte Carlo simulations<sup>54,58,74</sup>. In the presence of large strain, the potential is more washboard-like, with high ridges tracking the zig-zag direction and deep minima, again centered at the hexagon centers, but with a reduced energy barrier between them. The evolution of these coordination effects with strain are more apparent when normalizing deviations of the potential between their minimum and maximum values as seen in Fig. 12, where again we have

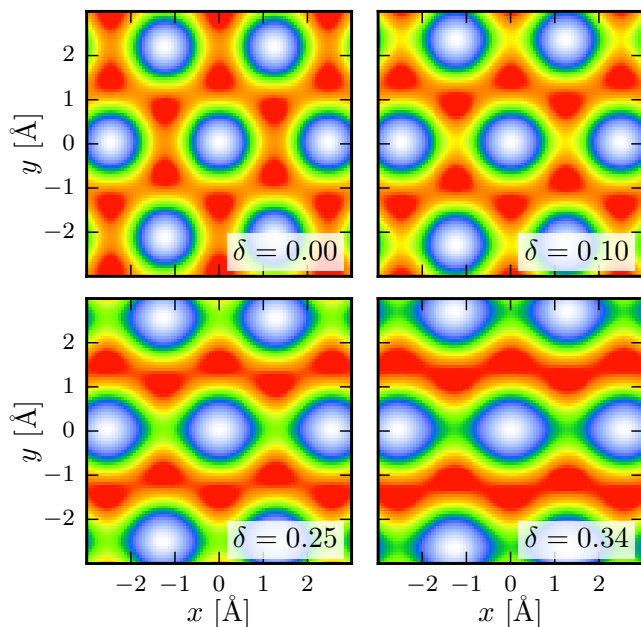


FIG. 12. (Color online) The Lennard-Jones potential  $U(x, y, r_m)$  for different values of the strain parameter  $\delta$  for a helium adatom located at fixed  $z = r_m$  above the graphene sheet where  $r_m(\delta) \simeq 2.635, 2.663, 2.768, 2.951$  Å is the strain dependent position of the minimum for  $\delta = 0.0, 0.1, 0.25, 0.34$  respectively. Each panel has been independently normalized such that the color scale ranges from  $\min_{x,y} U(x, y, r_m)$  (white) to  $\max_{x,y} U(x, y, r_m)$  (red).

fixed  $z = r_m(\delta)$ . The valley-to-peak difference in the potential increases from approximately 36 K for  $\delta = 0$  to 49 K for  $\delta = 0.25$  while the energy barriers between minima are systematically reduced along the zig-zag troughs.

If we increase the fixed height above the sheet and set it to the strain independent constant  $z = 2\sigma_0 = 5.48$  Å we find very different behavior as seen in Fig. 13. The location with respect to the lattice of peaks and valleys has now reversed, with the hexagon center always representing the maxima in the potential. While the variations in the potential are suppressed as  $z$  increases:  $\Delta U(z = 2\sigma_0, \delta = 0.0) \simeq 0.27$  mK and  $\Delta U(z = 2\sigma_0, \delta = 0.25) \simeq 1.8$  mK, the nearly 600% increase demonstrates the large range of mechanical tunability of vdW interactions in this system. We note that the distance  $z = 2\sigma_0$  corresponds to the approximate location above the graphene sheet where a second layer of helium is adsorbed<sup>54,74</sup> whose properties are still under debate<sup>50,58</sup>.

In summary, we have found that in order to reproduce the increase in the vdW attraction between a helium atom and a deformed graphene surface at large distances computed within Lifshitz theory, it is necessary to employ strain-dependent Lennard-Jones parameters. At short distances, these modified parameters in conjunction with the deformed lattice structure produce a highly anisotropic, yet weakened adsorption potential with min-

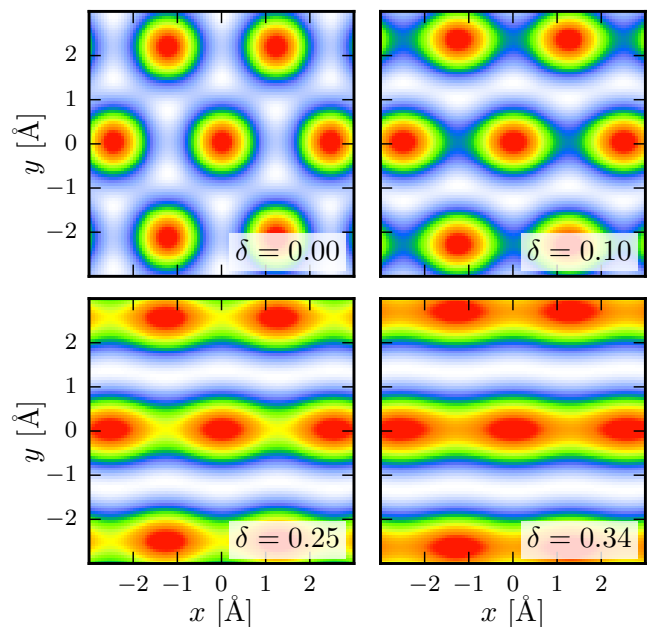


FIG. 13. The Lennard-Jones potential  $U(x, y, 2\sigma_0)$  for different values of the strain parameter  $\delta$  for a helium adatom located at  $z = 2\sigma_0 = 5.48$  Å above the graphene sheet.

ima pushed to higher energies at a location further above the graphene compared to the unstrained case. For the largest strains we considered (35%), the potential minima is pushed to nearly 3 Å above the substrate. However, in contrast to weaker strains, the depth of the potential well is slightly greater than that for isotropic graphene. At these extreme deformations, there is some ambiguity in the relationship between the velocity anisotropy  $v_y/v_x$  and the strain percentage  $\delta$  which requires an extrapolation procedure. This uncertainty in combination with a reduction in confidence of our fitting method in this high-strain regime, indicates that a closer look at the short distance potential is warranted. This can be accomplished via a first principles determination of the dispersion energy.

#### D. *Ab initio* calculations for coronene

In this section, we calculate from *ab initio* methods the interaction potential of a single He atom situated at a distance  $z$  above the center of an aromatic molecule, which represents a reasonable model for the near-field interaction of the atom with a graphene plane. The interaction of neutral atoms and molecules with graphene is dominated by dispersion terms, leading to van der Waals-type potentials, as discussed above. The *ab initio* evaluation of dispersion terms is delicate, requiring accurate treatment of the correlation energy<sup>75,76</sup>. Two methods are considered reliable enough for this determination<sup>75</sup>: Møller-Plesset<sup>77</sup> or coupled cluster<sup>78</sup>. Whereas the latter

is considered of higher precision, its computational cost is prohibitive for larger molecular clusters and provides relatively small quantitative gains. Thus, we have performed calculations using the 2nd order Møller-Plesset perturbative approach which captures about 95% of the correlation energy<sup>75</sup>.

All calculations were performed in Gaussian 09<sup>79</sup> using the Pople-type<sup>80</sup> 6-31++G(d,p) basis set which includes diffusion of all orbitals and polarization functions d for carbon and p for helium. For the aromatic molecules representing graphene, we utilized coronene ( $C_{24}H_{12}$ , lower inset, Fig. 14) or strained coronene, with the carbon atoms situated at positions given in Eqs. (21)–(22), i.e., no geometry optimizations were performed on the aromatic carbons which would have eliminated the strain (the positions of the hydrogen terminators were optimized in each configuration). The energy of the system was computed for various values of the distance  $z$  between the He atom and the aromatic plane, and the asymptotic energy for  $z \rightarrow \infty$  was removed as a baseline (obtained by extrapolation of the energies for  $z = 10, 15, 20$ , and  $30 \text{ \AA}$ ).

The results for the interaction potential of He on strained coronene are shown in Fig. 14. The upper inset shows the dependence of this potential on the size of the aromatic compound. We find, in agreement with the calculations of Section IV C, that strain has two dominant and connected effects on the helium adsorption potential: the potential minima is pushed outwards from the sheet (as compared to isotropic molecules) causing the attraction strength to be diminished. Within our first principles numerical calculations, this trend is monotonic with increasing strain, further supporting the hypothesis that the previously employed fitting procedure breaks down for highly deformed graphene lattices. The absolute value of the energy of the adsorption potential minima differs substantially between Figs. 10 and 14 due to the presence of hydrogen terminators necessary for chemical stability.

## V. CONCLUSIONS AND OUTLOOK

In conclusion, we have analyzed in detail the van der Waals potential of three atoms (He, H, and Na) with uniaxially strained graphene ranging from weak to moderately strong. While these atoms have very different static polarizabilities (Na being the most polarizable and He the least) and characteristic frequencies, leading to very different potential strengths, the overall dependence of their van der Waals potential on graphene strain is quite similar. The potential is sensitive to strain and always increases, which can be traced back to the enhanced graphene polarization. Since the enhanced polarization also leads to increased screening of the Coulomb potential, as described by Eqs. (4), (5) and (12), the exact value of the van der Waals potential increase reflects the delicate balance between higher polarization and screening. Our calculations show that enhance-

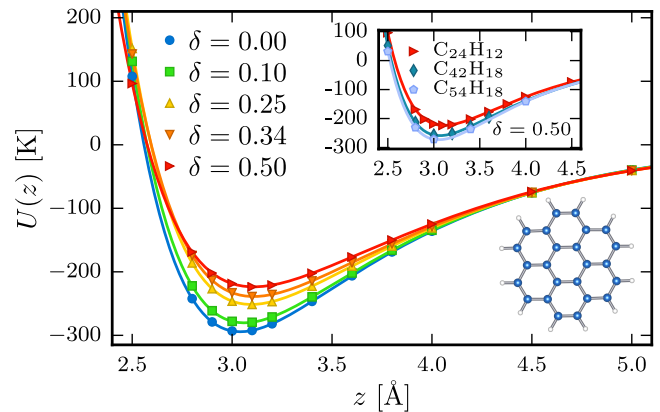


FIG. 14. (Color online) Adsorption potential for helium above (centered) a single strained coronene ( $C_{24}H_{12}$ ) molecule (lower right) calculated in the 2nd order Møller-Plesset<sup>77</sup> approximation using a 6-31++G(d,p) basis set<sup>80</sup>. Upper left: dependence of the adsorption potential on molecular size calculated for  $\delta = 0.50$  in coronene ( $C_{24}H_{12}$ ) hexabenzocoronene ( $C_{42}H_{18}$ ), and circumcoronene ( $C_{54}H_{18}$ ) (same axes as main panel). Similar size-dependence is observed for lower strains.

ment of the van der Waals potential can be as high as 100% for strong strain  $\delta \approx 35\%$ . For such large values we always keep in mind that the strain is in the armchair direction to ensure that the system remains semi-metallic (i.e. in the anisotropic Dirac fermion “universality class”). While it is unrealistic to expect that graphene itself can be used in this extreme regime, the development of artificial anisotropic graphene-like lattices as well the continuous stream of discoveries in the field of 2D atomic crystals could provide a potentially exciting and fruitful playground for the phenomena we describe in this paper. As mentioned in Section I, examples of such anisotropic systems include graphene superlattices<sup>13–16</sup>, tunable honeycomb optical lattices<sup>17</sup>, and molecular graphene<sup>18</sup>. Additional systems of interest could include atomically thin  $MoS_2$ <sup>12,81</sup> which exhibits strain-sensitive band structure<sup>82–84</sup>, as well as graphene on hexagonal boron nitride (h-BN), with a superlattice of spontaneous strain fields and strong electron correlation effects<sup>85–87</sup>. Analysis of these and other 2D materials requires extensions of the present work in several directions, such as inclusion of spectral gap, spin-orbit coupling, and gauge fields induced by more complicated strain configurations, among others<sup>12</sup>.

We have applied our results on the strain dependence of the van der Waals interaction to the problem of quantum reflection, finding that it can be significantly suppressed by strain. Pragmatically, this implies that cold atoms on strained graphene-based lattices can approach the surface and thus experience strong inelastic scattering (usually accompanied by emission of flexural phonons in the substrate). In this regime, dissipative many-body phenomena<sup>64</sup> become of great importance as strain is ap-

plied; these are by themselves complex theoretical problems which we leave for future studies.

Finally, we have explored the effects of mechanical strain on the helium-graphene adsorption potential near the surface, finding that it can be drastically modified. By matching the results of long-distance continuum calculations of the van der Waals interaction with an effective sum over two-body interactions for He above a strained graphene lattice, we have independently determined phenomenological Lennard-Jones parameters for the system, finding agreement with common values used for the helium-carbon interaction. As strain is increased, the parameters  $\varepsilon$  and  $\sigma$  for the two-body interaction grow monotonically. While this causes an increase in attraction far from the sheet, the strength of the resulting many-body adsorption potential for helium near the surface is reduced. The resulting locations of potential minima reflect the anisotropy of the deformed lattice and are pushed to larger distances above the sheet, causing weaker adsorption with increased strain. This trend was confirmed via *ab initio* calculations of a single helium atom above aromatic nanographene molecules.

Mechanically tuning the helium-graphene adsorption potential presents a fundamentally new approach to the problem of engineering novel low dimensional liquid phases, providing a method to inhibit classical wetting and promote collective behavior. The formation of connected adsorption potential valleys in Fig. 12 for 25%

strain may allow for adatoms to minimize their kinetic energy by spatially delocalizing along them, offering a mechanism that may favor anisotropic first layer superfluidity at low temperature. At smaller (and more experimentally realistic) values of strain, the first layer may remain commensurate, but the second adsorbed layer, which should be both anisotropic and weakly bound, would be an ideal candidate to form a two dimensional quantum liquid. This possibility is particularly exciting in light of the fact that the exact nature of the second layer of helium adsorbed on a *graphite* surface is still under debate<sup>48,88</sup> with recent heat capacity measurements indicating the possibility of an exotic quantum hexatic state<sup>50</sup>. The introduction of a mechanical strain into the arsenal of experimental tuning parameters may help to uncover and confirm the existence of this and other predicted quantum liquid phases.

## VI. ACKNOWLEDGMENTS

We are grateful to Dennis Clougherty for numerous stimulating discussions related to the subject of this work and we acknowledge M. Cole for his insights into the adsorption of helium on graphite. The research of V. N. Kotov was supported by the U.S. Department of Energy (DOE) grant DE-FG02-08ER46512.

- 
- <sup>1</sup> Geim, A. K. and Grigorieva, I.V., *Nature* **499**, 419 (2013).  
<sup>2</sup> V. M. Pereira, A. H. Castro Neto, and N. M. R. Peres, *Phys. Rev. B* **80**, 045401 (2009).  
<sup>3</sup> R. M. Ribeiro, V. M. Pereira, N. M. R. Peres, P. R. Bridgdon, and A. H. C. Neto, *New J. Phys.* **11**, 115002 (2009).  
<sup>4</sup> S.-M. Choi, S.-H. Jhi, and Y.-W. Son, *Phys. Rev. B* **81**, 081407 (2010).  
<sup>5</sup> F. M. D. Pellegrino, G. G. N. Angilella, and R. Pucci, *Phys. Rev. B* **82**, 115434 (2010).  
<sup>6</sup> F. M. D. Pellegrino, G. G. N. Angilella, and R. Pucci, *Phys. Rev. B* **81**, 035411 (2010).  
<sup>7</sup> C. Lee, X. Wei, J. W. Kysar, and J. Hone, *Science* **321**, 385 (2008).  
<sup>8</sup> Z. H. Ni, T. Yu, Y. H. Lu, Y. Y. Wang, Y. P. Feng, and Z. X. Shen, *ACS Nano* **2**, 2301 (2008).  
<sup>9</sup> K. S. Kim, Y. Zhao, H. Jang, S. Y. Lee, J. M. Kim, K. S. Kim, J. H. Ahn, P. Kim, J. Choi, and B. H. Hong, *Nature* **457**, 706 (2009).  
<sup>10</sup> D. C. Elias, R. R. Nair, T. M. G. Mohiuddin, S. V. Morozov, P. Blake, M. P. Halsall, A. C. Ferrari, D. W. Boukhvalov, M. I. Katsnelson, A. K. Geim, and K. S. Novoselov, *Science* **323**, 610 (2009).  
<sup>11</sup> V. M. Pereira and A. H. Castro Neto, *Phys. Rev. Lett.* **103**, 046801 (2009).  
<sup>12</sup> B. Amorim, A. Cortijo, F. de Juan, A. Grushin, F. Guinea, A. Gutiérrez-Rubio, H. Ochoa, V. Parente, R. Roldán, P. San-Jose, J. Schiefele, M. Sturla, and M. Vozmediano, *Physics Reports* **617**, 1 (2016).  
<sup>13</sup> C.-H. Park, L. Yang, Y.-W. Son, M. L. Cohen, and S. G. Louie, *Phys. Rev. Lett.* **101**, 126804 (2008).  
<sup>14</sup> C.-H. Park, L. Yang, Y.-W. Son, M. L. Cohen, and S. G. Louie, *Nature Phys.* **4**, 213 (2008).  
<sup>15</sup> S. Rusponi, M. Papagno, P. Moras, S. Vlaic, M. Etzkorn, P. M. Sheverdyeva, D. Pacilé, H. Brune, and C. Carbone, *Phys. Rev. Lett.* **105**, 246803 (2010).  
<sup>16</sup> J. Sun, H. A. Fertig, and L. Brey, *Phys. Rev. Lett.* **105**, 156801 (2010).  
<sup>17</sup> L. Tarruell, D. Greif, T. Uehlinger, G. Jotzu, and T. Esslinger, *Nature* **483**, 302 (2012).  
<sup>18</sup> K. K. Gomes, W. Mar, W. Ko, F. Guinea, and H. C. Manoharan, *Nature* **483**, 306 (2012).  
<sup>19</sup> Sernelius, B. E., *Europhys. Lett.* **95**, 57003 (2011).  
<sup>20</sup> M. Bordag, B. Geyer, G. L. Klimchitskaya, and V. M. Mostepanenko, *Phys. Rev. B* **74**, 205431 (2006).  
<sup>21</sup> G. L. Klimchitskaya and V. M. Mostepanenko, *Phys. Rev. B* **87**, 075439 (2013).  
<sup>22</sup> M. Bordag, I. V. Fialkovsky, D. M. Gitman, and D. V. Vassilevich, *Phys. Rev. B* **80**, 245406 (2009).  
<sup>23</sup> G. Gómez-Santos, *Phys. Rev. B* **80**, 245424 (2009).  
<sup>24</sup> J. Sarabadani, A. Naji, R. Asgari, and R. Podgornik, *Phys. Rev. B* **84**, 155407 (2011).  
<sup>25</sup> B. E. Sernelius, *Phys. Rev. B* **85**, 195427 (2012).  
<sup>26</sup> G. L. Klimchitskaya, U. Mohideen, and V. M. Mostepanenko, *Rev. Mod. Phys.* **81**, 182 (2009).  
<sup>27</sup> J. F. Dobson, T. Gould, and G. Vignale, *Phys. Rev. X* **4**, 021040 (2014).

- <sup>28</sup> J. F. Dobson, A. White, and A. Rubio, *Phys. Rev. Lett.* **96**, 073201 (2006).
- <sup>29</sup> D. Drosdoff and L. M. Woods, *Phys. Rev. B* **82**, 155459 (2010).
- <sup>30</sup> A. Sharma, P. Harnish, A. Sylvester, V. N. Kotov, and A. H. C. Neto, *Phys. Rev. B* **89**, 235425 (2014).
- <sup>31</sup> E. Lifshitz and L. Pitaevskii, *Statistical Physics*, Part 2 (Pergamon Press, 1980).
- <sup>32</sup> I. Dzyaloshinskii, E. Lifshitz, and L. Pitaevskii, *Advances in Physics* **10**, 165 (1961).
- <sup>33</sup> A. Sharma, V. N. Kotov, and A. H. Castro Neto, *Phys. Rev. B* **87**, 155431 (2013).
- <sup>34</sup> K. S. Novoselov, A. K. Geim, S. V. Morozov, D. Jiang, Y. Zhang, S. V. Dubonos, I. V. Grigorieva, and A. A. Firsov, *Science* **306**, 666 (2004).
- <sup>35</sup> K. S. Novoselov, A. K. Geim, S. V. Morozov, D. Jiang, M. I. Katsnelson, I. V. Grigorieva, S. V. Dubonos, and A. A. Firsov, *Nature* **438**, 197 (2005).
- <sup>36</sup> Geim, A. K. and Novoselov, K. S., *Nature Mat.* **6**, 183 (2007).
- <sup>37</sup> A. K. Geim, *Science* **324**, 1530 (2009).
- <sup>38</sup> A. H. Castro Neto, F. Guinea, N. M. R. Peres, K. S. Novoselov, and A. K. Geim, *Rev. Mod. Phys.* **81**, 109 (2009).
- <sup>39</sup> V. N. Kotov, B. Uchoa, V. M. Pereira, F. Guinea, and A. H. Castro Neto, *Rev. Mod. Phys.* **84**, 1067 (2012).
- <sup>40</sup> J. F. Babb, G. L. Klimchitskaya, and V. M. Mostepanenko, *Phys. Rev. A* **70**, 042901 (2004).
- <sup>41</sup> Y. V. Churkin, A. B. Fedortsov, G. L. Klimchitskaya, and V. A. Yurova, *Phys. Rev. B* **82**, 165433 (2010).
- <sup>42</sup> E. V. Blagov, G. L. Klimchitskaya, and V. M. Mostepanenko, *Phys. Rev. B* **71**, 235401 (2005).
- <sup>43</sup> M. Chaichian, G. L. Klimchitskaya, V. M. Mostepanenko, and A. Tureanu, *Phys. Rev. A* **86**, 012515 (2012).
- <sup>44</sup> S. Ribeiro and S. Scheel, *Phys. Rev. A* **88**, 042519 (2013).
- <sup>45</sup> L. Bruch, M. Cole, and E. Zaremba, *Physical Adsorption: Forces and Phenomena* (Dover Publications, 2007).
- <sup>46</sup> M. Bretz and J. Dash, *Phys. Rev. Lett.* **26**, 963 (1971).
- <sup>47</sup> G. Zimmerli, G. Mistura, and M. Chan, *Phys. Rev. Lett.* **68**, 60 (1992).
- <sup>48</sup> D. S. Greywall, *Physical Review B* **47**, 309 (1993).
- <sup>49</sup> J. G. Dash, M. Schick, and O. E. Vilches, *Surf. Sci.* **299-300**, 405 (1994).
- <sup>50</sup> S. Nakamura, K. Matsui, T. Matsui, and H. Fukuyama, (2014), 1406.4388.
- <sup>51</sup> F. Abraham and J. Broughton, *Phys. Rev. Lett.* **59**, 64 (1987).
- <sup>52</sup> M. Pierce and E. Manousakis, *Phys. Rev. B* **59**, 3802 (1999).
- <sup>53</sup> P. Corboz, M. Boninsegni, L. Pollet, and M. Troyer, *Phys. Rev. B* **78**, 245414 (2008).
- <sup>54</sup> M. Gordillo and J. Boronat, *Phys. Rev. Lett.* **102**, 085303 (2009).
- <sup>55</sup> M. C. Gordillo, C. Cazorla, and J. Boronat, *Phys. Rev. B* **83**, 121406 (2011).
- <sup>56</sup> M. C. Gordillo and J. Boronat, *Phys. Rev. B* **85**, 195457 (2012).
- <sup>57</sup> M. C. Gordillo and J. Boronat, *J. Low Temp. Phys.* **171**, 606 (2013).
- <sup>58</sup> J. Happacher, P. Corboz, M. Boninsegni, and L. Pollet, *Phys. Rev. B* **87**, 094514 (2013).
- <sup>59</sup> M. Boninsegni and S. Moroni, *Phys. Rev. E* **86**, 056712 (2012).
- <sup>60</sup> W. E. Carlos and M. W. Cole, *Surf. Sci.* **91**, 339 (1980).
- <sup>61</sup> A. Derevianko, S. G. Porsev, and J. F. Babb, *Atomic Data and Nuclear Data Tables* **96**, 323 (2010).
- <sup>62</sup> T. E. Judd, R. G. Scott, A. M. Martin, B. Kaczmarek, and T. M. Fromhold, *New J. Phys.* **13**, 083020 (2011).
- <sup>63</sup> G. Dufour, A. Gérardin, R. Guérout, A. Lambrecht, V. V. Nesvizhevsky, S. Reynaud, and A. Y. Voronin, *Phys. Rev. A* **87**, 012901 (2013).
- <sup>64</sup> D. P. Clougherty and W. Kohn, *Phys. Rev. B* **46**, 4921 (1992).
- <sup>65</sup> T. A. Pasquini, Y. Shin, C. Sanner, M. Saba, A. Schirotzek, D. E. Pritchard, and W. Ketterle, *Phys. Rev. Lett.* **93**, 223201 (2004).
- <sup>66</sup> T. A. Pasquini, M. Saba, G.-B. Jo, Y. Shin, W. Ketterle, D. E. Pritchard, T. A. Savas, and N. Mulders, *Phys. Rev. Lett.* **97**, 093201 (2006).
- <sup>67</sup> B. S. Zhao, G. Meijer, and W. Schllkopf, *Science* **331**, 892 (2011).
- <sup>68</sup> H. Friedrich, G. Jacoby, and C. G. Meister, *Phys. Rev. A* **65**, 032902 (2002).
- <sup>69</sup> H. Friedrich and J. Trost, *Phys. Rep.* **397**, 359 (2004).
- <sup>70</sup> M. Oobatake and T. Ooi, *Prog. of Theor. Phys.* **48**, 2132 (1972).
- <sup>71</sup> D. Boda and D. Henderson, *Mol. Phys.* **106**, 2367 (2008).
- <sup>72</sup> G. Derry, D. Wesner, W. Carlos, and D. Frankl, *Surf. Sci.* **87**, 629 (1979).
- <sup>73</sup> W. E. Carlos and M. W. Cole, *Phys. Rev. Lett.* **43**, 697 (1979).
- <sup>74</sup> Y. Kwon and D. M. Ceperley, *Phys. Rev. B* **85**, 224501 (2012).
- <sup>75</sup> C. Cramer, *Essentials of Computational Chemistry: Theories and Models* (Wiley, 2013).
- <sup>76</sup> R. J. Bartlett, *Ann. Rev. Phys. Chem.* **32**, 359 (1981).
- <sup>77</sup> C. Møller and M. S. Plesset, *Phys. Rev.* **46**, 618 (1934).
- <sup>78</sup> J. A. Pople, M. Head-Gordon, and K. Raghavachari, *The Journal of Chemical Physics* **87** (1987).
- <sup>79</sup> M. J. Frisch, G. W. Trucks, H. B. Schlegel, G. E. Scuseria, M. A. Robb, J. R. Cheeseman, G. Scalmani, V. Barone, B. Mennucci, G. A. Petersson, H. Nakatsuji, M. Caricato, X. Li, H. P. Hratchian, A. F. Izmaylov, J. Bloino, G. Zheng, J. L. Sonnenberg, M. Hada, M. Ehara, K. Toyota, R. Fukuda, J. Hasegawa, M. Ishida, T. Nakajima, Y. Honda, O. Kitao, H. Nakai, T. Vreven, J. A. Montgomery, Jr., J. E. Peralta, F. Ogliaro, M. Bearpark, J. J. Heyd, E. Brothers, K. N. Kudin, V. N. Staroverov, R. Kobayashi, J. Normand, K. Raghavachari, A. Rendell, J. C. Burant, S. S. Iyengar, J. Tomasi, M. Cossi, N. Rega, J. M. Millam, M. Klene, J. E. Knox, J. B. Cross, V. Bakken, C. Adamo, J. Jaramillo, R. Gomperts, R. E. Stratmann, O. Yazyev, A. J. Austin, R. Cammi, C. Pomelli, J. W. Ochterski, R. L. Martin, K. Morokuma, V. G. Zakrzewski, G. A. Voth, P. Salvador, J. J. Dannenberg, S. Dapprich, A. D. Daniels, . Farkas, J. B. Foresman, J. V. Ortiz, J. Cioslowski, and D. J. Fox, "Gaussian 09 Revision E.01," Gaussian Inc. Wallingford CT 2009.
- <sup>80</sup> W. J. Hehre, R. F. Stewart, and J. A. Pople, *J. Chem. Phys.* **51**, 2657 (1969).
- <sup>81</sup> K. F. Mak, C. Lee, J. Hone, J. Shan, and T. F. Heinz, *Phys. Rev. Lett.* **105**, 136805 (2010).
- <sup>82</sup> A. Castellanos-Gomez, R. Roldán, E. Cappelluti, M. Buscema, F. Guinea, H. S. J. van der Zant, and G. A. Steele, *Nano Lett.* **13**, 5361 (2013).
- <sup>83</sup> H. J. Conley, B. Wang, J. I. Ziegler, R. F. Haglund, S. T. Pantelides, and K. I. Bolotin, *Nano Lett.* **13**, 3626 (2013).

- <sup>84</sup> H. Peelaers and C. G. Van de Walle, Phys. Rev. B **86**, 241401 (2012).
- <sup>85</sup> B. Sachs, T. O. Wehling, M. I. Katsnelson, and A. I. Lichtenstein, Phys. Rev. B **84**, 195414 (2011).
- <sup>86</sup> P. San-Jose, A. Gutiérrez-Rubio, M. Sturla, and F. Guinea, Phys. Rev. B **90**, 075428 (2014).
- <sup>87</sup> P. San-Jose, A. Gutiérrez-Rubio, M. Sturla, and F. Guinea, Phys. Rev. B **90**, 115152 (2014).
- <sup>88</sup> Y. Shibayama, H. Fukuyama, and K. Shirahama, J. Phys.: Conf. Ser. **150**, 032096 (2009).